JOURNAL OF CATALYSIS 155, 238–248 (1995)

Surface Organometallic Chemistry on Metals: Preparation of Bimetallic Catalysts by Controlled Hydrogenolysis of $Sn(n\text{-}C_4H_9)_4$ on a Ni/SiO_2 Catalyst

P. Lesage,* O. Clause,† P. Moral,‡ B. Didillon,† J. P. Candy,* and J. M. Basset*

*Laboratoire de Chimie Organométallique de Surface, UMR CNRS-CPE 9986, CPE, 43 Bd du 11 Novembre 1918, 69100 Villeurbanne, France; †Institut Français du Pétrole, 1 et 4 Avenue de Bois-Préau, 92506 Rueil-Malmaison Cédex, France; and ‡Institut de Recherches sur la Catalyse, 2 Avenue Albert Einstein, 69626 Villeurbanne Cédex, France

Received October 24, 1994; revised March 2, 1995

Selective hydrogenolysis of $Sn(n\text{-}C_4H_9)_4$ on a Ni/SiO_2 catalyst has been carried out at various temperatures and at various coverages of the metallic surface by the organotin(IV) compound. The surface reaction was followed by chemical analysis of the gaseous and surface products, electron microscopy, infrared spectroscopy, magnetic measurements, and EXAFS measurements. At room temperature, and in the absence of metallic particles, $Sn(n\text{-}C_4H_9)_4$ is simply physisorbed on the silica surface and can be easily extracted by *n*-heptane. In the presence of metallic Ni, and provided that the amount of Sn introduced represents less than ca. a monolayer of the metallic surface, hydrogenolysis of $Sn(n\text{-}C_4H_9)_4$ occurs exclusively on the Ni particles, as evidenced by STEM–EDAX measurements, infrared spectroscopy, and EXAFS measurements. Analysis of the gaseous products evolved at increasing temperatures, infrared measurements, and EXAFS measurements indicate a stepwise cleavage of Sn–alkyl bonds. At temperatures lower than 323 K, there is formation of relatively stable surface organometallic fragments which can be formulated as $Ni_s[Sn(n\text{-}C_4H_9)_x]_y$ in which "Ni_s" represents surface nickel atoms ($x = 2, 3$). The stoichiometry of the surface reaction leading to stable surface organometallic fragments depends both on the surface coverage (y) of the nickel particle by the organometallic compound and on the temperature of the hydrogenolysis. For the sample obtained after hydrogenolysis at 323 K for 10 h and for a Sn/Ni_s ratio of 0.5, an average of 2.5 butyl groups remain on the surface. The EXAFS experiments (at the Sn *K*-edge) carried out on such a sample show that adsorbed Sn is surrounded on average by 2.5 light backscatterers (very probably C type) and by 1.3 heavy backscatterers (most probably Ni). Various possible structures have been proposed, taking into account the results of the analytical and EXAFS data, as well as the magnetic and chemisorption measurements. For reaction temperatures greater than 373 K, all butyl groups are hydrogenolysed mainly as butane. STEM–EDAX experiments show that, provided that the amount of Sn introduced is lower than a monolayer of the Ni_s, the signal of Sn is always associated with that of Ni, indicating the lack of migration of tin to silica. Electron microscopy indicates that the average metallic particle size on the surface increases by a value of about 1.5 nm. For a Sn/Ni_s ratio of 0.5, EXAFS studies show that each "naked" tin atom is surrounded by 4 Ni atoms or less, suggesting that tin atoms have not migrated into the nickel particles. Magnetic measurements suggest that each tin atom has then the same magnetic effect as 4.5 chemisorbed hydrogen atoms.

1. INTRODUCTION

Surface organometallic chemistry (SOMC) is a relatively new field of chemistry devoted to the study of the reactivity of organometallic complexes with surfaces (1). The complexes may be those of main group elements, transition metals, lanthanides, or actinides (2–4). The surfaces may be those of highly divided inorganic oxides (5, 6), or those of zero-valent metallic particles (7–10). In the latter case, the field is defined as surface organometallic chemistry on metals (SOMC/M) (11). The nature of the metallic surface may be that of a highly dispersed metallic particle, supported or unsupported, or even that of a single crystal. The new catalytic materials obtained by SOMC/M can be divided into two groups, depending on whether or not some organometallic fragments remain on the surface:

(i) There are no remaining organometallic fragments on the surface; the high selectivity observed with these bimetallic catalysts, presumably but not necessarily alloys, has been ascribed to the simple concept of site isolation (7). According to this concept, the catalytically "active" transition metal atom is surrounded by catalytically "inactive" Sn atoms so that no possibility of side reactions (for example, those involving dimetallacycle intermediates (12)) can occur. However, the degree of control of the "coordination sphere" of the "active metal atom" in an alloy is limited: it is restricted to the composition of the alloy and to the nature of the so-called inactive metal.

(ii) There is a remaining organometallic fragment on the surface; it is then theoretically possible to control at an atomic and molecular level the coordination sphere of the

0021-9517/95 $12.00

active metal atom with this organometallic fragment. By changing at will the steric and electronic properties of this organometallic fragment, it should be possible to influence the chemo-stereo- and/or regio-selectivity of a variety of reactions catalyzed by metallic surfaces (13–17).

Recently, we have demonstrated that it is possible to graft tin alkyl fragments onto the surface of rhodium particles supported on silica by selective hydrogenolysis of $Sn(n\text{-}C_4H_9)_4$ on this material (18). When the amount of tin introduced represents less than a monolayer on the metallic surface, the reaction occurs almost exclusively at the metallic surface and not on the silica surface. Interestingly, the new catalytic material obtained by this route exhibits unexpected catalytic properties of chemoselectivities: whereas rhodium alone does not present any chemoselectivity in the hydrogenation of olefinic aldehydes, the rhodium particles covered by tin–alkyl fragments are both very active and very selective for the hydrogenation of the aldehydic function (16). It was therefore of interest to see whether or not other transition metals can accommodate on their surface stable tin alkyl fragments and under which chemical and/or thermal conditions this can occur. This article reports results which demonstrate for the first time that it is also possible to graft organotin fragments, namely $Sn(n\text{-}C_4H_9)_x$, onto the surface of Ni particles supported on silica. These organometallic fragments are also obtained by selective hydrogenolysis of $Sn(n\text{-}C_4H_9)_4$ on the metallic surface of silica-supported Ni particles.

2. EXPERIMENTAL

2.1. *Monometallic-Supported Ni Catalyst*

The preparation of the monometallic catalyst has been described elsewhere (19). The silica support (Aerosil 200 $m^2\ g^{-1}$) was purchased from Degussa. $Ni(NH_3)_6(OH)_2$ is obtained by dissolution of $Ni(NO_3)_2 \cdot 6H_2O$ in a concentrated ammonia solution. The Ni is grafted onto silica by cationic exchange between $[Ni(NH_3)_6]^{2+}$ ions and surface $\equiv Si\text{–}O^-NH_4^+$ groups by stirring a slurry of the silica and the $[Ni(NH_3)_6]^{2+}$ for 10 h. After filtration, the surface complex obtained is then decomposed by calcination at 673 K under a mixture of flowing nitrogen/oxygen (5/1), reduced under flowing H_2 at 673 K and then passivated at 298 K under a flowing oxygen–nitrogen mixture (3/100). Analysis of the nickel or tin content was achieved after treatment with HNO_3 + HCl and then HF. After dissolution of the sample, quantitative analysis was carried out by atomic absorption. The accuracy for nickel and tin was close to 2 and 5%, respectively.

2.2. *Chemisorption Measurements*

Gas adsorption measurements were carried out at room temperature using conventional Pyrex volumetric adsorption equipment. The vacuum (10^{-6} mbar) was achieved with a liquid-nitrogen-trapped mercury diffusion pump. The equilibrium pressure was measured with a Texas Instrument gauge (pressure range 0–1000 mbar with an accuracy of 0.1 mbar). The catalyst sample was placed in a Pyrex flow-through cell to allow reduction in flowing hydrogen at 773 K. After reduction, the cell was sealed and the sample was outgassed at 523 K for 2 h under vacuum before hydrogen chemisorption measurements. The amount of hydrogen adsorbed by the catalyst was determined from the decrease in gas pressure.

At room temperature and under an equilibrium pressure of 200 mbar, it was assumed that each nickel surface atom (Ni_s) adsorbs one hydrogen atom, as already established by several workers (20, 21). Metal dispersion ($D = Ni_s/Ni$) was calculated from H_2 uptake. Average crystallite diameter (d) was evaluated using the equation d (nm) = $0.971/D$, based on the assumption that the metal particles are spherical and of uniform size (22).

2.3. *Hydrogenolysis of $Sn(n\text{-}C_4H_9)_4$ on Reduced Ni Particles ($Ni_s\text{-}H/SiO_2$)*

This reaction was performed in the same apparatus as described above. After reduction under flowing H_2, the sample was sealed under H_2 and then kept at room temperature under 30 mbar of H_2. This catalyst is described hereafter as Ni_s-H catalyst. The desired amount of $Sn(n\text{-}C_4H_9)_4$ was then carefully introduced into the reactor via a septum, without any contact with air. The reaction was performed at various temperatures: 298, 323, 373, and 423 K. The gases evolved during the reaction were trapped at liquid nitrogen temperature in another part of the apparatus, to avoid possible feedback of the gases onto the catalytic surface and prevent further hydrogenolysis. After various times (t) of reaction, the reactor was isolated and the temperature of the cold part was raised to room temperature. The gases evolved during the reaction time (t) were qualitatively and quantitatively analyzed by GC and volumetric measurements. At the end of the reaction, the solid was washed with n-heptane and the amount of unreacted $Sn(n\text{-}C_4H_9)_4$ was measured by GC.

In order to determine the stoichiometry of the surface reaction, a careful quantitative analysis of the reactants (H_2 and $Sn(n\text{-}C_4H_9)_4$) and gaseous products was carried out. The reaction between a given amount of $Sn(n\text{-}C_4H_9)_4$ and H_2 with a known amount of $Ni_s\text{-}H/SiO_2$ was performed in a closed vessel. For a Sn/Ni_s ratio fo 0.5 and a slight excess of H_2, all $Sn(n\text{-}C_4H_9)_4$ reacted. Therefore, one can assume the general chemical equation

$$\underbrace{H_2}_{(a)} + \underbrace{Sn(n\text{-}C_4H_9)_4}_{(b)} + \underbrace{(Ni_s\text{-}H)}_{(c)} \rightarrow \underbrace{(Ni_s\text{-}H)}_{(d)} + \underbrace{[(Ni_s)_zSn(n\text{-}C_4H_9)_x]}_{(b)} + \underbrace{C_4H_9}_{(e)} + \underbrace{H_2}_{(f)} \quad [1]$$

The quantity of $Sn(n\text{-}C_4H_9)_4$ introduced (b) was controlled. Careful measurement of the initial amount of gaseous hydrogen (a), the initial amount of adsorbed hydrogen (c), the total amount of butane evolved (e), and the final amount of gaseous hydrogen (f), allow us to calculate the amount of adsorbed hydrogen at the end of the reaction (d) on the new catalytic material: $d = c + 2a\text{-}e\text{-}2f$. The number ($z$) of surface nickel atoms available for grafting on one $Sn(n\text{-}C_4H_9)_x$ fragment was easily obtained by $z = (c\text{-}d)/b$. The values obtained for $y = 0.5$ (y = Sn/Ni_s) after reaction at 323 or 423 K are reported in Table 1.

2.4. *Magnetic Measurements*

The magnetization of the samples was measured in an electromagnet (field up to 21 kOe) at room temperature using the Weiss extraction method (23). The system was calibrated using unsupported pure nickel. The sample was prepared following the same procedure as described previously. At the desired step of the reaction, the reactor was sealed in order to completely isolate the sample and the magnetization of the sample was measured. The degree of reduction was calculated from saturation data taken on the reduced monometallic catalyst. Two metallic particle sizes were evaluated from magnetization data at high and low magnetic fields (d_1 and d_2, respectively). The average diameter of the nickel particles was deduced from the simple equation: $d = (d_1 + d_2)/2$.

2.5. *Electron Microscopy*

Conventional transmission electron microscopy (CTEM) and scanning transmission electron spectroscopy (STEM–EDAX) were performed using JEOL 100 CX and Vacuum Generator HB5 electron microscopes, respectively. CTEM was used to obtain histograms of metallic particle size of the catalysts. STEM experiments were carried out to identify and to locate Sn and Ni on the silica surface.

2.6. *Infrared Spectroscopy*

Infrared spectra were obtained with a Nicolet 10 MX-1 Fourier transform instrument. All the experiments were carried out under a controlled atmosphere with strict exclusion of air, oxygen, and moisture. The samples (self-supporting wafers) were placed in a sample holder which could move inside a closed reactor from the treatment position (located in an oven) to the analysis position (located between two CaF_2 windows in the infrared beam). Infrared spectroscopy was used to evaluate the number of alkyl groups present on the surface during the hydrogenolysis reaction of $Sn(n\text{-}C_4H_9)_4$ on Ni_s/SiO_2. This was achieved by considering the absorbance of the ν(C–H) band at 2960 cm^{-1}. The introduction of $Sn(n\text{-}C_4H_9)_4$ was carried out under a controlled atmosphere via a syringe through a septum connected to the IR cell.

2.7. *EXAFS Analysis*

The EXAFS measurements were performed at the LURE synchrotron radiation facility using the X-ray beam emitted by the DCI storage ring (positron energy, 1.85 eV; ring current 300 mA). The spectra were recorded in the transmission mode at room temperature using a Si(311) double-crystal monochromator and two Ar-filled ionization chambers as detectors. EXAFS cells, about 1 cm thick, with sealed Kapton windows were used as sample holders. The samples were prepared as described above at the desired temperature under H_2 in a glass reactor connected to the EXAFS cell. The powdered samples were transferred under argon to the EXAFS cells, which were then sealed. The edge jumps ranged from 0.5 to 1.0 eV and the total absorption beyond the Sn K-edge ranged from 2 to 2.5 eV. The energies were scanned with 3 eV steps starting from 100 eV below the edge up to 800 eV beyond the edge. The $\Delta E/E$ resolution was estimated to be approximately 4×10^{-4}.

3. RESULTS

3.1. *Characterization of the Monometallic Material: Ni/SiO_2*

Ni/SiO_2-supported monometallic catalyst was prepared with a metal loading of 6.55%. The particle size distribu-

TABLE 1

Stoichiometry of the Reaction between $Sn(n\text{-}C_4H_9)_4$ and Ni_s-H for Sn/Ni_s = 0.5 for Two Reaction Temperatures

	Coefficients of Eq. [1][a]								
T (K)	a	b	c	d	e	f	Ratio d/c	x^b	z^b
323	63.5 ± 1	54 ± 1	108 ± 1	58 ± 2	143 ± 1	17 ± 1	0.53 ± 2	2	1.1
423	212 ± 1	54 ± 1	108 ± 1	49 ± 1	226 ± 1	134 ± 1	0.45 ± 2	0	1.1

Note. a, b, c, d, e, and f are the Coefficients of Eq. [1].

[a] a, b, e, and f are expressed in μmol/g; c and d are expressed in μatom/g.

[b] $x = C_4/Sn$; $z = (c - d)/b$.

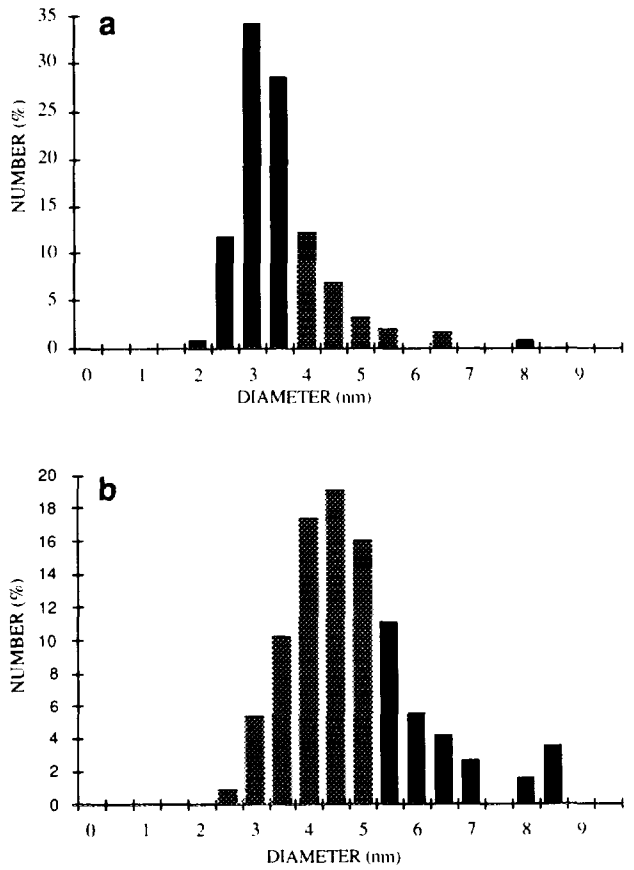

FIG. 1. Particle size distribution, on the surface, of the various catalysts deduced from CTEM: (a) Ni/SiO_2, (b) $Ni-Sn/SiO_2$ after hydrogenolysis of $Sn(n\text{-}C_4H_9)_4$ at 573 K for 5 h.

tion of this Ni/SiO_2 catalyst has been determined by CTEM analysis. A typical histogram is given in Fig. 1. The distribution is rather narrow, with an average diameter (d) of 4.0 nm. Using the formula $D = 0.971/d$ (22) an estimated dispersion of 0.24 was obtained.

Chemisorption of H_2 was used as an indirect method to determine metal particle size. The isotherms were measured at 298 K under hydrogen pressures ranging from 0 to 300 mbar. As seen in Fig. 2, there is a plateau for hydrogen pressures higher than ca. 50 mbar. Under these conditions, the amount of gas adsorbed on the support is negligible. The accepted stoichiometry of 1 $H_{atom}/Ni_{s\,(atom)}$ was assumed at the above-mentioned equilibrium pressure. The resulting dispersion (0.22) is in good agreement with the value obtained from CTEM analysis (0.24).

The degrees of reduction were calculated from the magnetization at saturation data. They were taken on the reduced (723 K under flowing hydrogen) and desorbed (523 K for 2 h *in vacuo*) monometallic catalysts. They were estimated to be close to 100% (24). Two metallic particle sizes were evaluated from magnetization data at high (d_1) and low (d_2) magnetic fields (d_1 = 3.9 nm and

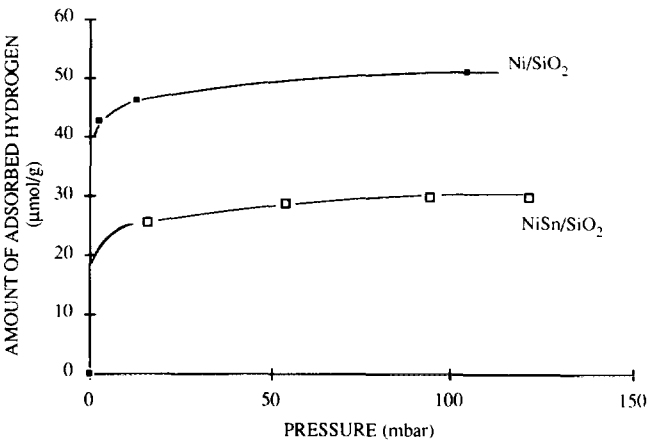

FIG. 2. Isotherms of H_2 adsorption on (a) the starting Ni/SiO_2 and (b) on the $NiSn/SiO_2$. Sn/Ni_s = 0.5.

d_2 = 5.9 nm). The average diameter deduced from the equation $d = (d_1 + d_2)/2$ was 4.9 nm, in quite good agreement with the value obtained from CTEM (4 nm). In summary, three independent methods give similar results for the metallic particle size, namely 4.5 ± 0.5 nm.

3.2. *Hydrogenolysis of $Sn(n\text{-}C_4H_9)_4$ on $Ni_s\text{-}H/SiO_2$*

3.2.1. Stoichiometry of the Hydrogenolysis Reaction as a Function of Temperature. The amount of fixed tin as well as the analysis of the gases evolved for the reaction at various temperatures and for three different Sn/Ni_s ratios are reported in Figs. 3–5 and Table 2.

For any reaction temperatures lower than 373 K, butane is the only gas evolved. For reaction temperatures higher than 373 K, the major product is still butane, but small quantities of butenes (ca. 8%), propane (ca. 8%), ethane (ca. 2.1%), and methane (ca. 2.1%) are observed.

Figures 3–5 show that the amount of evolved gas

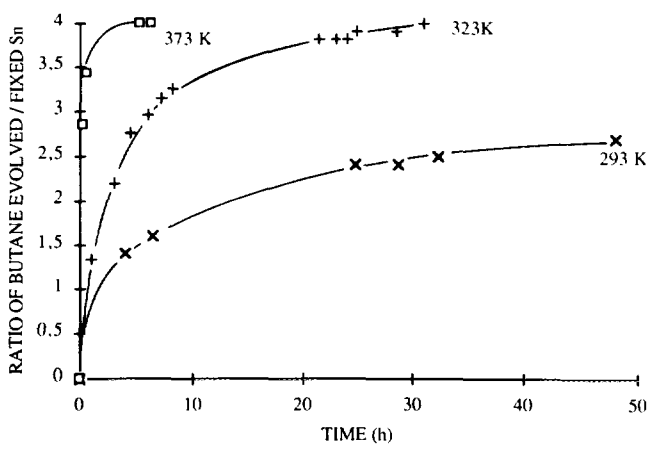

FIG. 3. Amount of butane evolved during the reaction at various temperatures between $Ni\text{-}H/SiO_2$ and $Sn(n\text{-}C_4H_9)_4$. Sn/Ni_s = 0.2.

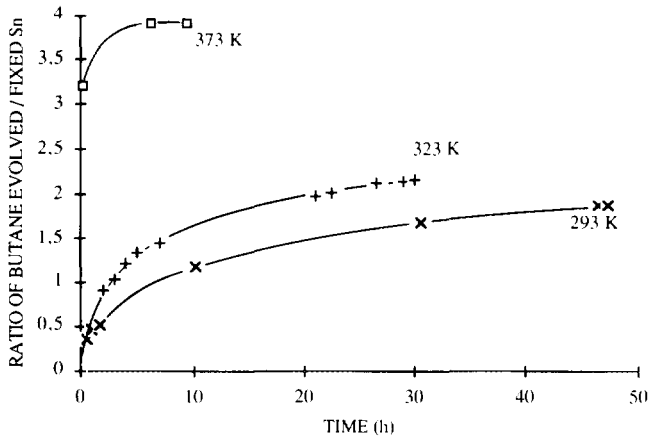

FIG. 4. Amount of butane evolved during the reaction at various temperatures between Ni/SiO_2 and $Sn(n\text{-}C_4H_9)_4$. $Sn/Ni_s = 0.5$.

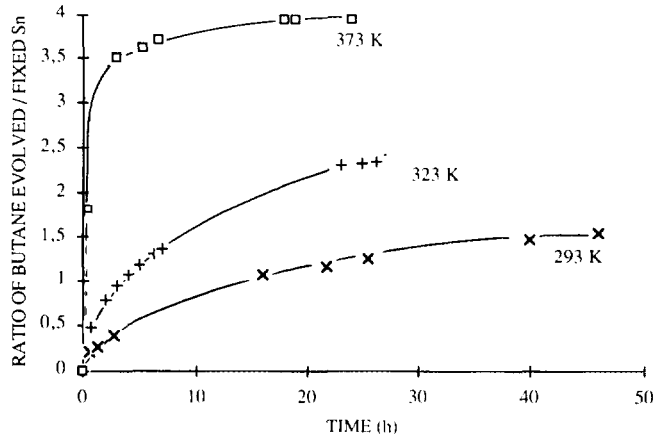

FIG. 5. Amount of butane evolved during the reaction at various temperatures between Ni/SiO_2 and $Sn(n\text{-}C_4H_9)_4$. $Sn/Ni_s = 1$.

reaches a plateau after a certain time of interaction. This phenomenon is observed regardless of the Sn/Ni_s ratio. After reaching these equilibria, washing the catalyst with *n*-heptane did not remove any significant amount of unreacted $Sn(n\text{-}C_4H_9)_4$. Therefore, all $Sn(n\text{-}C_4H_9)_4$ introduced was fixed on the catalyst surface. This result is confirmed by the data of Table 2: Within experimental error, the amount of tin introduced at the beginning of the experiment is equal to the amount of grafted tin at the end of the experiment. The amount of gas evolved depends on temperature and on the Sn/Ni_s ratio: For a given temperature, the lower the Sn/Ni_s ratio, the higher the amount of butane evolved. For example, at 323 K, the tin complex is fully dealkylated for a Sn/Ni_s ratio of 0.2 but only partially dealkylated for Sn/Ni_s ratios greater than 0.5 (compare Figs. 3 and 4). At 298 K, there are clearly some butyl groups remaining on the catalyst surface, even after 50 h of reaction (see Figs. 3–5). A new material which can be described by the general formula $Ni_s[Sn(n\text{-}C_4H_9)_x]_y$ with $1.5 < x < 2.5$ for $0.2 < y < 1$ is thus obtained. At 323 K and for $y > 0.5$, almost two butyl groups remain on the surface even after 30 h of reaction, while for $y = 0.2$, all the butyl groups are removed after ca. 20 h. At 373 K, regardless of the coverage of the metallic surface, all the butyl groups of the starting tin complex are removed after less than 10 h.

These data indicate clearly that, for a given temperature, the coverage of the nickel surface atoms by the organometallic fragment determines the overall stoichiometry of the hydrogenolysis:

(i) At high surface coverage there is incomplete hydrogenolysis, and the surface organometallic fragments are stable, at least at low temperature (298 K).

(ii) At low coverage of the Ni surface, the organometallic fragment is fully dealkylated even at low temperature. Steric crowding is less important around the grafted organotin compound and there are enough nickel atoms to achieve full hydrogenolysis of the alkyl chains.

This interpretation of the data is probably oversimplified since it is quite reasonable to assume that the hydrogenolysis of the organometallic fragment will occur more specifically on certain crystallographic planes or defects. Therefore the coverage is not the only parameter to consider if one wishes to fully understand this aspect of surface organometallic chemistry on metals.

The determination of the stoichiometry of the surface

TABLE 2

Comparison between the Amount of $Sn(n\text{-}C_4H_9)_4$ Introduced, Sn/Ni_s (intr) and the Amount of Grafted Tin Sn/Ni_s (anal), after 50 Hours of Reaction at Various Temperatures

	Temperature (K)					
	298	373	298	423	298	373
Sn/Ni_s (intr)	0.20	0.20	0.50	0.50	1.0	1.0
Sn/Ni_s (anal)[a,b]	0.30	0.26	0.55	0.49	0.90	1.1

[a] The catalyst was washed with *n*-heptane to remove any unreacted $Sn(n\text{-}C_4H_9)_4$.

[b] The Sn/Ni_s ratio was determined by chemical analysis, but the accuracy of these measurements is ±0.1.

TABLE 3

Magnetic Effect of Tin Atoms or Fragments Observed during Reaction at Increasing Temperatures between $Sn(n\text{-}C_4H_9)_x$ and Hydrogen-Covered Ni_s/SiO_2

	Sample number[a]						
	1	2	3	4	5	7	8
Temperature (K)	298	298	298	323	373	573	723
M_i (a.u.)	233	193	175	175	124	106	100
$\theta_{H_{ads}}$	0	1	0.5	0.5	0.5	0.5	0.5
$y(Sn/Ni_s)$	—	—	0.5	0.5	0.5	0.5	0.5
$x(C_4/Sn)$	—	—	2.5	1.5	0	0	0
$M_f/Sn(\mu_H)$	—	—	1.9	1.9	4.4	5.3	5.6

[a] For sample designation, see text.

reaction has been achieved by considering the mass balance of reactants and products at equilibrium. The following equations can be observed at two temperatures (see Experimental and Table 3):

$$0.5\ Sn(n\text{-}C_4H_9)_4 + (Ni_s\text{-}H) \xrightarrow{323\ K} 0.5\ (Ni_s\text{-}H) + 0.5[Sn(n\text{-}C_4H_9)_2(Ni_s)] + C_4H_{10}$$

$$0.5\ Sn(n\text{-}C_4H_9)_4 + (Ni_s\text{-}H) \xrightarrow{373\ K} 0.5\ (Ni_s\text{-}H) + 0.5[SnNi_s] + 2\ C_4H_{10}.$$

The relative amount of hydrogen remaining on the catalyst after reaction at 323 and 423 K (Table 1) ($\theta_{H_{ads}} = d/c$) was close to 0.5. This suggests that each organometallic fragment cancels the chemisorptive property of the same number of nickel atoms as each atom of hydrogen.

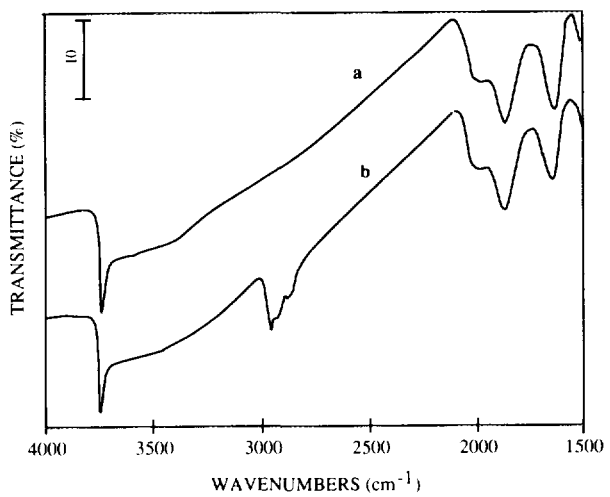

FIG. 6. Infrared spectra corresponding to (a) the monometallic reduced Ni_s-H/SiO_2 catalyst and (b) to the same catalyst after reaction with $Sn(n\text{-}C_4H_9)_4$ at 298 K for 50 h.

3.2.2. Infrared spectroscopy. Infrared spectroscopy was used to follow the hydrogenolysis of $Sn(n\text{-}C_4H_9)_4$ on the catalyst Ni_s-H/SiO_2. Figure 6 presents spectra corresponding to the monometallic reduced Ni_s-H/SiO_2 catalyst (a) and to the same catalyst after reaction with $Sn(n\text{-}C_4H_9)_4$ at 298 K for 50 h under hydrogen (b). The ν(OH) vibration of the silica support situated at 3748 cm^{-1} is not modified. Simultaneously, the ν(C–H) bands corresponding to the grafted alkyl chains are observed at 2960 $\nu_a(CH_3)$, 2928 $\nu_a(CH_2)$, 2878 $\nu_s(CH_3)$, and 2862 cm^{-1} $\nu(CH_2)_s$ (25). These results indicate that when reduced metallic Ni particles are present on silica, $Sn(n\text{-}C_4H_9)_4$ reacts with the metal particles preferentially.

On silica, $Sn(n\text{-}C_4H_9)_4$ reacts with the silanols at about 423 K to give the well-defined compound >Si–O–$Sn(n\text{-}C_4H_9)_3$ which has been fully characterized (28). Interestingly, with this grafted organotin compound, the alkyl chains are interacting *inter alia* with the remaining silanols via hydrogen bonding. This interaction, which can be demonstrated both by CP-MAS ^{13}C NMR and by infrared spectroscopy, causes important modifications of the ν(OH) vibrations of the silanols (drastic broadening and a low-frequency shift of the ν(OH) bands) and a significant chemical shift of the ^{13}C resonance of the δ carbon (see Scheme 1). Interestingly, this interaction does not seem to occur to a great extent when the organometallic fragment is situated on the metallic particle.

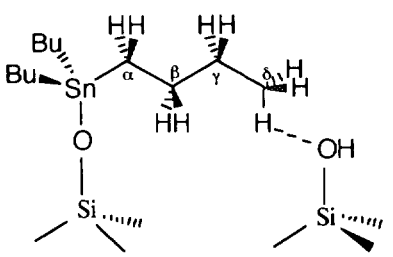

SCHEME 1

The variation in the intensity of $\nu(CH_x)$ bands corresponding to the grafted alkyl chains and to the gas phase during the reaction with $Sn(n\text{-}C_4H_9)_4$ at 298 K is shown in Fig. 7. Clearly, there is a rapid decrease in the intensity of the bands attributed to the grafted organometallic fragment and, simultaneously, a rapid increase in the intensity of the bands characteristic of the gaseous butane.

As seen in Fig. 7, a temperature of 423 K is needed to fully remove the butyl groups from the metallic surface. To summarize this infrared study, it appears that the organometallic compound does not react at low temperature with the silanol groups. This can be evidenced by the presence of the $\nu(CH)$ bands of the alkyl chains and by the absence of modification of the $\nu(OH)$ bands of the silica. Above 423 K, the alkyl chains are hydrogenolyzed and appear in the gas phase (as hydrocarbons).

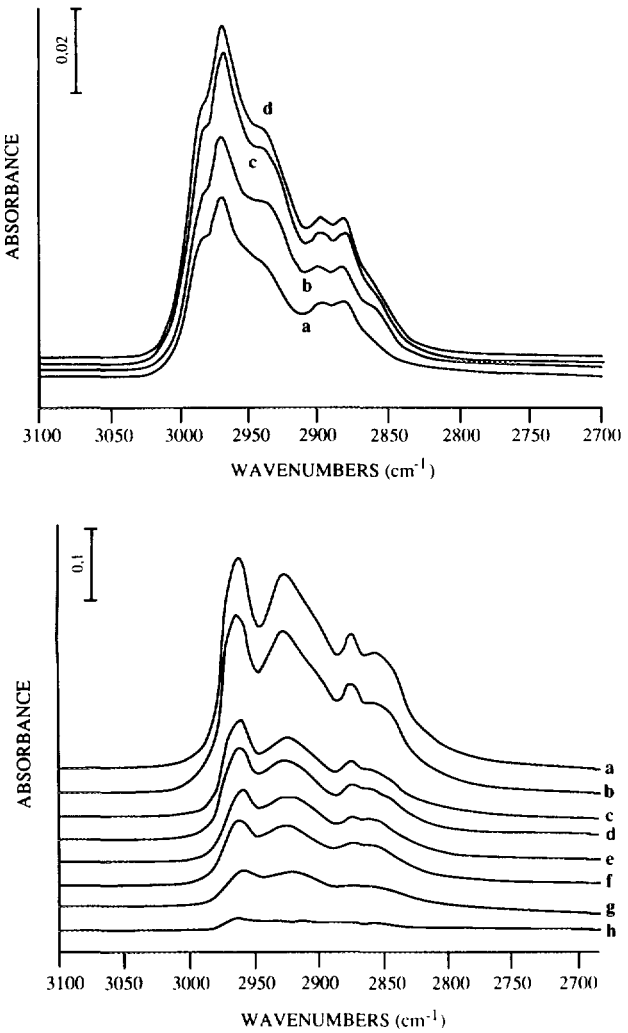

FIG. 7. Variation in the transmittance of the $\nu(CH_x)$ bands corresponding to the grafted alkyl chains (below) and to the gas phase (above) during the hydrogenolysis reaction of $Sn(n\text{-}C_4H_9)_4$ at 298 K, during 1h45, a, 3h15, b, 18h30, c, 50h, d, 90h, e, and 323 K, f, 373K, g, and 423 K, h.

3.2.3. Magnetic measurements. Magnetic measurements, when applied to dispersed nickel particles, can give useful information both on the morphology of the reduced particles (degree of reduction, metal particle size) and on the nature of adsorbed species (23). Saturation magnetization (M_s) was calculated by plotting the magnetization M against $1/H$ (H is the magnetic field) and extrapolating to $1/H = 0$. Variations of saturation magnetization ΔM_s occurring during chemisorption of simple molecules such as hydrogen are usually expressed in μ_3 per adsorbed molecule. The magnetic effect of one adsorbed molecule (x) is then expressed by $\mu_x = k\Delta M_s/q$, where q is the amount of adsorbed molecules. In order to easily compare the results, we take the magnetic effect of one adsorbed hydrogen atom as unity: this assumption means that each adsorbed atom of hydrogen cancels the magnetization of one nickel atom. The corresponding value is denoted μ_H.

Various samples were prepared and their magnetizations at saturation (M_s) were taken at room temperature.

—Sample (1) was a monometallic catalyst reduced at 723 K and desorbed at 523 K *in vacuo*. It is denoted $Ni^{(0)}/SiO_2$.

—Sample (2) was obtained from sample (1) after treatment under 30 mbar of H_2 and is denoted Ni_sH/SiO_2.

—Samples (3), (4), (5), (6), (7), and (8) were obtained by reaction between sample (2) and a desired amount of $Sn(n\text{-}C_4H_9)_4$ corresponding to the ratio $Sn/Ni_s = 0.5$. The reaction was performed under 30 mbar H_2 for 30 h at 298, 323, 373, 473, 573, and 723 K for samples (3), (4), (5), (6), (7), and (8), respectively. The amount of butane evolved during these reactions (C_4/Sn) and the relative amount of hydrogen remaining adsorbed on the catalyst ($\theta_{H_{ads}}$) was quantitatively determined.

Variations in the magnetization at saturation (M_i) and in the amount of butane evolved with reaction temperature are reported in Table 3. Clearly, the magnetization at saturation of the starting sample decreases in several steps: The first step is due to the formation of the nickel hydride ($\theta = 1$). We assume that each surface hydrogen atom cancels the magnetization of one surface nickel atom. The second step occurs when $Sn(n\text{-}C_4H_9)_4$ is allowed to react with the hydrogen-covered surface. When approximately 2 ± 0.5 butyl groups have reacted to give butane and a surface organometallic fragment $Ni_s[Sn(n\text{-}C_4H_9)_x]_y$ ($x = 2 \pm 0.5$; $y = 0.5$) there is a new decay of the saturation magnetization. This decay is moderate and will be used to estimate the number of nickel atoms magnetically perturbed by each organometallic fragment (*vide infra*). The third step is observed when all the butyl groups have been evolved as butane and the nickel surface is covered by the naked tin atoms. One can see easily that this decrease in magnetization of the nickel particle is the strongest: the number of nickel atoms magnetically perturbed by each tin atom is quite large.

If one takes into account the magnetic effect of the remaining adsorbed hydrogen, it is possible to calculate the magnetic (M_f/Sn) effect of each grafted Sn(n-C_4H_9)$_x$ fragment or naked tin. The results are reported in Table 3 from which it is seen that each grafted organometallic fragment ($1 < x < 3$) has a magnetic effect of ca. 2 μ_H and each naked tin has a magnetic effect of ca. 4.5 to 6 μ_H depending on the temperature of reaction.

To a rough approximation one may be tempted to conclude that each tin organometallic fragment cancels the magnetic susceptibility of two nickel atoms. When this tin organometallic fragment is fully dealkylated, the number of nickel atoms affected by this tin atom increases drastically. For a reaction temperature of 373 K, the number of these nickel atoms is about 4.5, suggesting that the tin atoms are located on the outer layer of the particles. For reaction temperatures greater than 573 K, each naked tin atoms cancels the magnetism of more than 6 nickel atoms as if there was formation of an alloy in which each tin atom is surrounded on average by several nickel atoms. Let us recall that at such a Sn/Ni ratio (12%) tin–nickel alloys are still magnetic (29).

3.2.4. Electron microscopy. The particle size distribution of the bimetallic catalyst obtained by reaction between Ni_s-H/SiO_2 and Sn(n-C_4H_9)$_4$ (Sn/Ni_s = 0.5) at 473 K has been determined by CTEM analysis. A typical histogram is given in Fig. 1b. The distribution is rather narrow, with an average particle diameter d of 5 nm. If we compare this histogram with the histogram of the starting monometallic catalyst, there is an increase in the size of each of the metallic particles, rather than an increase in the metallic size via a sintering effect.

Scanning transmission electron microscopy performed on more than 500 metallic particles of the same bimetallic solid as above confirm that tin and nickel are located in each metallic particle with the same atomic ratio as expected from the amount of Sn(n-C_4H_9)$_4$ introduced and confirmed by elemental analysis. No isolated tin atoms on the silica surface are observed.

3.2.5. Extended X-ray absorption fine structure. The adsorption of metal ions onto alumina using metal ions as local microprobes has been recently studied by EXAFS (26). By analogy, the adsorption of Sn(n-C_4H_9)$_4$ on reduced Ni/SiO_2 systems has been followed by EXAFS at the SnK-edge. Three samples have been successively investigated: sample (a), Ni-free silica impregnated with Sn(n-C_4H_9)$_4$; sample (b), obtained by interaction between Ni/SiO_2 and Sn(n-C_4H_9)$_4$ (Sn/Ni_s = 0.5) under hydrogen (30 mbar) at 323 K for 10 h; and sample (c), obtained by interaction between Ni/SiO_2 and Sn(n-C_4H_9)$_4$ (Sn/Ni_s = 0.5) under hydrogen (30 mbar) at 423 K for 5 h.

k^3-Weighted Fourier transforms without phase correction were performed over the $3.5 < k < 11.5$ range after multiplication by a Hanning window; see Fig. 8a. Background subtraction, normalization, and Fourier transforms were performed using the UWXAFS analysis package developed at the University of Washington (27). The Fourier-transformed EXAFS spectra, without phase correction, of samples (a), (b) and (c) are reported in Fig. 8. For sample (a), the presence of close backscatters at R value lower than 2 Å, probably the Cα of the butyl groups are observed. Upon heating, the nearest backscattering peak is broadened and shifted to R value close to 2 Å, as shown in Fig. 8b. For sample (c), a narrow peak is observed at a distance higher than 2 Å, which is probable attributable to Ni or Sn backscatters.

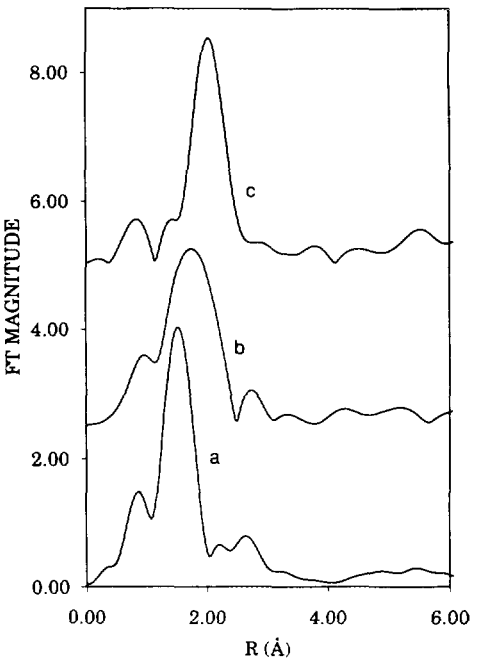

FIG. 8. Fourier transforms (k^3 weighted; without phase correction) of (a) $SnBu_4$; (b) sample obtained by interaction between Ni/SiO_2 and $SnBu_4$ (Sn/Ni_s = 0.5) under hydrogen at 50°C for 10 h; (c) sample obtained by interaction between Ni/SiO_2 and $SnBu_4$ (Sn/Ni_s = 0.5) under hydrogen at 423 K for 10 h.

Theoretical Sn···C, Sn···Ni, and Sn···Sn phase shift and amplitude functions were calculated using the FEFF5 program developed at the University of Washington (27). Due to the large difference between their atomic numbers, Ni and Sn backscatterers can be readily distinguished by EXAFS. Conversely, O and C backscatterers are very difficult to separate. In agreement with the preliminary results showing that Sn(n-C_4H_9)$_4$ does not react at room temperature with silica in the absence of Ni particles (under the conditions specified for the preparation of samples (b) and (c)), the presence of carbon (rather than oxygen) backscatterers around the grafted tin atoms was assumed. The fits were performed both on the real and imaginary parts of the Fourier transforms over a $1 < R < 2.9$ Å

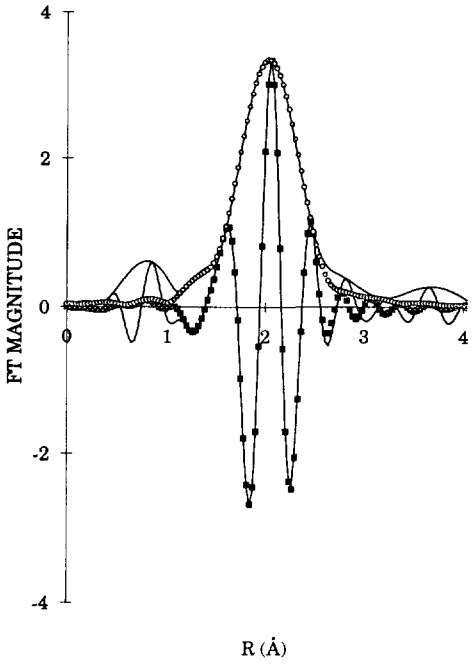

FIG. 9. Imaginary part and magnitude of Fourier transform (solid lines; k^3 weighted; without phase correction) of the sample obtained by interaction between Ni/SiO_2 and $SnBu_4$ ($Sn/Ni_s = 0.5$) under hydrogen at 423 K for 10 h. The results of EXAFS analysis obtained with the best calculated coordination parameters are shown with marks (■, imaginary part; ○, magnitude). The fits were performed over the 1.1- to 2.9-Å R range.

range (see Fig. 9). For the fitting procedures no constraints were introduced on the distances, coordination numbers, Debye–Waller factors, or energy shifts.

The EXAFS signal of sample (a), consisting of silica-supported $Sn(n\text{-}C_4H_9)_4$, was easily fitted with 4 C backscatterers located at 2.12 Å around the tin atoms; see Table 4.

For sample (c), the peak at 2.2 Å (uncorrected distance value; see Fig. 8c) could be unambiguously attributed to Ni backscatterers, with a coordination number of 3.2. A minor contribution of C backscatterers was taken into account to fit correctly a shoulder visible in the main peak of the Fourier transform, shown in Fig. 8c. The total coordination number around the tin atoms in sample (c) remained close to 4, a value much lower than that expected for a true alloy of the same composition (ca. 10). As expected, the EXAFS analysis of sample (b) indicated a tin environment intermediate between those observed in samples (a) and (c). Average values of 2.5 and 1.3 were found for the C and Ni coordination numbers, respectively. In all samples, the total coordination number ($N_C + N_{Ni}$) was approximately 4. Thus, the Sn–C were progressively replaced for Sn–Ni bonds when the butyl groups were evolved.

4. DISCUSSION

In this paper we have studied the selective hydrogen olysis of $Sn(n\text{-}C_4H_9)_4$ by silica-supported Ni. The metallic phase of the starting Ni material is composed of particles of zero-valent Ni regularly distributed on the silica surface with a narrow distribution of particle sizes centered around 4 nm. The size of these particles has been confirmed by electron microscopy, magnetic measurements, and chemisorption of H_2. The zero oxidation state of the metallic particles has been determined by magnetic measurement.

At 298 K and under 30 mbar of hydrogen, $Sn(n\text{-}C_4H_9)_4$ reacts selectively with the nickel surface with formation of butane. After 50 h of reaction, and for a ratio $Sn(n\text{-}C_4H_9)_4$ introduced per Ni_s atoms lower than 0.9, the total quantity of $Sn(n\text{-}C_4H_9)_4$ introduced is fixed exclusively on the nickel surface and there is no evidence of silanol consumption. Evidence for such selective hydrogenolysis of the organotin complex on the nickel surface is given by a combination of several techniques, namely IR, STEM–EDAX, chemical analysis, magnetization measurements, and EXAFS at the Sn K-edge.

Clearly, some butyl groups remain on the nickel surface, as demonstrated by infrared measurements and by chemical analysis of the total amount of butane evolved at increasing temperatures. However, the situation is complex and several parameters play an important role.

TABLE 4

Structural Parameters of Samples (a)–(c) Determined by EXAFS at the Sn K-Edge[a]

Sample	Backscatterer	Coordination number	R(Å)	Debye–Waller factor σ (Å) × 10^3	Energy shifts ΔE_0 (eV)
(a)	C	4.4	2.12	3.3	−1.0
(b)	C	2.5	2.17	3.3	−3.0
	Ni	1.3	2.62	10.0	−3.0
(c)	C	0.8	2.16	9.0	−5.0
	Ni	3.2	2.58	10.8	−5.0

[a] The inaccuracies of the coordination numbers, distances, and Debye–Waller factors are ±20%, ±2% and ±20%, respectively.

The temperature and the coverage of the nickel surface atoms by the organometallic fragment determine the overall stoichiometry of the hydrogenolysis:

—at high surface coverage there is incomplete hydrogenolysis and the surface organometallic fragments are stable at least at low temperature (298 K);

—at low coverage of the Ni surface, the organometallic fragment is fully dealkylated even at low temperature (298 K).

There are probably several reasons that explain such behavior: steric crowding could occur at high coverage and prevent the alkyl chains from further hydrogenolysis on the surface. At low coverage, steric crowding is less important around the grafted organotin compound and there are enough nickel atoms to achieve full hydrogenolysis of the alkyl chains. The second parameter which should be mentioned is the effect of defects on the selectivity of the hydrogenolysis. It is probable that the degree of hydrogenolysis of the organometallic fragment depends on the nature of the exposed planes or defects (low coordination atoms at edges, steps, or corners). We do not know what the structure of the catalyst would be if the hydrogenolysis were to be performed under continuous-flow conditions.

The structure of the grafted organometallic fragment will obviously depend on the temperature and the degree of coverage of the nickel surface. Consequently, the formulae vary from sample to sample. For the sample obtained after reaction at 323 K for 10 h and for a Sn/Ni_s ratio of 0.5, almost 2.5 butyl groups remain on the surface. The EXAFS experiments carried out on such a sample show that adsorbed Sn is surrounded, on average, by 2.5 light backscatterers (very likely C atoms) and by 1.3 heavy backscatterers which must be, most probably, Ni atoms. To summarize the various analytical data, particularly the EXAFS data (2.5 C atoms at 2.17 Å and 1.3 Ni atom at 2.62 Å), one is tempted to propose the coexistence of at least two surface structures for this particular situation as depicted in Scheme 2:

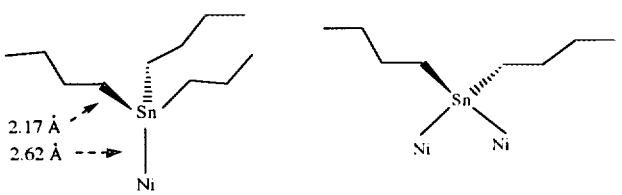

SCHEME 2

For the same sample, magnetic measurements indicate that, on average, the magnetic effect of each grafted organotin fragment is the same as that corresponding to two chemisorbed hydrogen atoms. Interestingly, careful measurements of the stoichiometry of the reaction suggest that each grafted organotin fragment occupied only one surface nickel atom.

For reaction temperatures greater than 373 K, all butyl groups are removed. STEM–EDAX experiments show that, provided that the amount of Sn introduced is lower than a monolayer of the Ni_s, the signal of Sn is always associated with that of Ni. No Sn signal is observed on the silica surface. Electron microscopy indicates that the average metallic particle size increases by a value of about 1.5 nm. Clearly, the tin atoms are located on or in the nickel particles. For a reaction of 5 h at a temperature of 423 K and for a Sn/Ni_s ratio of 0.5, EXAFS studies show that each naked tin atom is surrounded by less than 4 Ni atoms and magnetic measurements suggest that each tin atom has the same magnetic effect as 4.5 chemisorbed hydrogen atoms. For metallic particles of about 5 nm in diameter, if the tin atoms were located in the bulk of the metallic particles, the expected value for the number of nearest neighbors would be almost 7. Apparently after reaction at 373 K, the naked tin atoms are located on the surface or close to the surface of the nickel particles and not in the bulk. This is a reasonable assumption, considering that the number of tin atoms introduced is less than a monolayer of the surface and consequently less than a NiSn alloy.

ACKNOWLEDGMENTS

C. Leclercq is gratefully acknowledged for carrying out the electron microscope measurements, and G. A. Martin is acknowledged for help with the magnetic measurements.

REFERENCES

1. Basset, J. M., Gates, B. C., Candy, J. P., Choplin, A., Quignard, F., Leconte, M., and Santini, C., "Surface Organometallic Chemistry; Approaches to Surface Catalysis." Kluwer, Dordrecht, 1988.
2. Miura, H., Taguchi, H., Sugiyama, K., Matsuda, T., and Gonzalez, R. D., *J. Catal.* **124,** 194 (1990).
3. Izumi, Y., Asakura, K., and Iwasawa, Y., *J. Catal.* **127,** 631 (1991).
4. Yermakov, Y., Kuzetzov, B. N., and Ryndin, Y., *J. Catal.* **42,** 73 (1976).
5. Basset, J. M., Candy, J. P., Choplin, A., and Santini, C. A. T., *Catal. Today* **6,** 1 (1989).
6. Théolier, A., Choplin, A., Hilaire, L., d'Ornelas, L., Basset, J.-M., Hugo, R., Psaro, R., and Sourisseau, C., *Polyhedron* **2,** 119 (1983).
7. El Mansour, A., Candy, J. P., Bournonville, J. P., Ferretti, O. A., and Basset, J. M., *Angew. Chem.* **101,** 360 (1989).
8. Agnelli, M., Louessard, P., El Mansour, A., Candy, J. P., Bournonville, J. P., and Basset, J. M., *Catal. Today* **6,** 63 (1989).
9. Margitfalvi, J., Hegedüs, M., Góbölös, S., Kern-Tálas, E., Szedlacsek, P., Szabó, S., and Nagy, F., *in* "Proceedings, 8th International Congress on Catalysis, Berlin, 1984," p. 903. Dechema, Frankfurt-am-Main, 1984.
10. Travers, C., Bournonville, J. P., and Martino, G., *in* "Proceedings, 8th International Congress on Catalysis, Berlin, 1984," p. 891. Dechema, Frankfurt-am-Main, 1984.
11. Candy, J. P., Didillon, B., Smith, E. L., Shay, T. B., and Basset, J. M., *J. Mol. Catal.* **86,** 179 (1994).

12. Eloy, R., Leconte, M., Basset, J. M., Tanaka, K., and Tanaka, K.-I., *J. Am. Chem. Soc.* **110,** 275 (1988).
13. Didillon, B., Candy, J. P., Le Peltier, F., Sarrazin, P., Boitiaux, J. P., and Basset, J. M., U.S. Patent 5,235,106, August 10, 1993.
14. Didillon, B., Candy, J. P., Basset, J. M., and Bournonville, J. P. French Patent 89.13518, October 13, 1989; U.S. Patent 5.118.884, June 2, 1992.
15. Humblot, F., Candy, J. P., Santini, C., Didillon, B., Le Peltier, F., and Boitiaux, J. P., French Patent 92/09.429 July 28, 1992.
16. Didillon, B., Candy, J. P., El Mansour, A., Houtmann, C., and Basset, J.-M., *J. Mol. Catal.* **74,** 43 (1992).
17. Didillon, B., Le Peltier, F., Candy, J. P., Boitiaux, J. P., and Basset, J. M., *Prog. Catal.*, (1992).
18. Didillon, B., Houtman, C., Shay, T., Candy, J. P., and Basset, J. M., *J. Am. Chem. Soc.* **115,** 9380 (1993).
19. Agnelli, M., Candy, J. P., Basset, J. M., Bournonville, J. P., and Ferretti, O. A., *J. Catal.* **121,** 236 (1990).
20. Stockmeyer, R., Conrad, H. M., Renouprez, A., and Fouilloux, P., *Surf. Sci.* **49,** 549 (1975).
21. Martin, G. A., de Montgolfier, P., and Imelik, B., *Surf. Sci.* **36,** 675 (1973).
22. Bartholomew, C. H., and Pannell, R. B., *J. Catal.* **65,** 390 (1980).
23. Selwood, P. W., "Chemisorption and Magnetization" Academic Press, New York, 1976.
24. Martin, G. A., Imelik, B., and Prettre, M., *J. Chem. Phys.*, 66 (1969).
25. Marchand, A., Forel, M. T., Lebedeff, M., and Valade, M., *J. Organomet. Chem.* **26,** 69 (1971).
26. Paulhiac, J. L., and Clause, O., *J. Am. Chem. Soc.* **115,** 11, 602 (1993).
27. Rehr, J. J., Mustre de Leon, J., Zabinski, S. I., and Abers, R. C., *J. Am. Chem. Soc.* **113,** 5135 (1991).
28. Nedez, C., Théolier, A., Lefèbvre, F., Choplin, A., Basset, J.-M., and Joly, J.-F., *J. Am. Chem. Soc.* **115,** 772 (1993).
29. Bozorth, R. M., *in* "Ferromagnetism," p. 324. Van Nostrand, New York, 1953.